Nano Research 2013, 6(5): 356–364
DOI 10.1007/s12274-013-0312-z
Research Article

ISSN 1998-0124
CN 11-5974/O4

Redox-sensitive colorimetric polyaniline nanoprobes synthesized by a solvent-shift process

Jihye Choi[1,§], Yoochan Hong[2,§], Eugene Lee[3], Myeong-Hoon Kim[1], Dae Sung Yoon[2], Jinsuck Suh[3,4,5], Yongmin Huh[3,4,5], Seungjoo Haam[1,4] (✉), and Jaemoon Yang[3,4,6] (✉)

[1] *Department of Chemical and Biomolecular Engineering, Yonsei University, Seoul 120-749, Republic of Korea*
[2] *Department of Biomedical Engineering, Yonsei University, Wonju 220-710, Republic of Korea*
[3] *Department of Radiology, College of Medicine, Yonsei University, Seoul 120-752, Republic of Korea*
[4] *YUHS-KRIBB Medical Convergence Research Institute, Seoul 120-752, Republic of Korea*
[5] *Severance Biomedical Science Institute (SBSI), Seoul 120-752, Republic of Korea*
[6] *Severance Integrative Research Institute for Cerebral and Cardiovascular Diseases, Yonsei University Health System, Seoul 120-752, Republic of Korea*
[§] *These authors contributed equally to this work*

Received: 27 December 2012
Revised: 26 February 2013
Accepted: 24 March 2013

KEYWORDS
polyaniline,
solvent-shifting,
cancer,
colorimetric,
nanoprobe

ABSTRACT

We have synthesized water-stable polyaniline nanoparticles coated with tri-armed polyethylene glycol chains using a solvent-shift method and confirmed their colloidal size and aqueous solubility. Furthermore, we have demonstrated that the polyaniline nanoparticles can be doped with biological dopants to produce distinct color changes allowing the detection of live cancer cells.

Polyaniline (PAni) is a conducting polymer that has attracted recent interest because of its high conductivity, the reversibility of its oxidation/reduction processes, the facile controllability of its redox state by doping, and the varying colors of its different redox states [1–4]. These unique characteristics have allowed PAni to find a variety of applications in electronic devices, sensors, actuators, and batteries [5–7]. Furthermore, the rapid development of nanotechnology and nanoscience has led to efforts to synthesize nanostructures such as nanofibers, nanowires, and nanospheres [8, 9]. Nanospheres are particularly

Address correspondence to Seungjoo Haam, haam@yonsei.ac.kr; Jaemoon Yang, 177hum@yuhs.ac

interesting for optoelectronics and sensors due to their large surface area relative to nanofibers and nanowires [10]. Importantly, the globular nature of the nanospheres enhances their solubility in common solvents facilitating structural characterization [11]. For many applications, colloidal solubility and stability of PAni nanostructures in aqueous solutions are required to optimize the physiological (pharmaceuticals, cosmetics, plant, protection, nutrition) or technical (varnishes, printing inks, toners) actions [12]. However, the development of simple synthetic procedures for the fabrication of uniform PAni nanoparticles remains challenging because as-synthesized PAni appears to intrinsically form fibrillar and linear molecular structures. The few examples reported of the synthesis of PAni nanoparticles in aqueous solutions include the use of templates such as polystyrene spheres, hydroxyl alkyl cellulose, and salicylic acid assisted polymerization [13–15]. There remains a need for a practical and simple synthetic method that is capable of generating pure and water-soluble PAni nanoparticles in bulk quantities [16].

In our previous work, we prepared water-soluble PAni nanoparticles using a nanoemulsion method (volatile non-polar organic solvent emulsions in an aqueous solution) via a high energy process, such as ultrasonication, and subsequent removal of the organic solvent [17]. However, the poor solubility of PAni in weakly polar organic solvents, e.g., chloroform, induced a broad distribution of PAni nanoparticles with relatively large sizes (> 100 nm). Herein, we improve our method and formulate nanoparticles with smaller size and enhanced colloidal stability in biological media. We introduce a simple and quick process based on a solvent-shift method to fabricate the water-stable PAni nanoparticles (Scheme 1). With the solvent-shift process, hydrophobic molecules can be easily dispersed in aqueous media without a high energy step [18, 19]. Hydrophobic PAni was dissolved in a water-miscible polar aprotic solvent and subsequently mixed with water to displace the solvent. To increase the colloidal stability of nanoparticles, we used Tween 80, which is a surfactant that has tri-arm polyethylene glycol chains. We investigated the potential ability of the Tween 80-coated PAni (TPAni) nanoparticles to act as a colorimetric probe by transitioning the doped states at varying redox values and monitoring the resulting color changes. Finally, we evaluated the possibility of using TPAni nanoparticles as indicators to confirm the redox status of proliferating cancer cells [17].

To prepare water-stable TPAni nanoparticles via the solvent-shift method, PAni was first synthesized by a chemical oxidation polymerization method using a previously published protocol [17]. TPAni nanoparticles were then prepared by dissolving different amounts (10, 50, 100, and 300 mg) of PAni in the emeraldine base (EB) state in 1.5 mL of N-methyl-2-pyrrolidinone (NMP) [20]. This solution was added to 20 mL of an aqueous solution containing 200 mg of Tween 80. The mixture was vigorously stirred at room temperature for 24 h. After the reaction, TPAni nanoparticles were purified by centrifugation (15,000 rpm for 30 min) in triplicate and the precipitated TPAni nanoparticles were dispersed in deionized water and excess surfactants were removed by a dialysis (molecular weight cut off: 25,000 Da). The colloidal size was confirmed using dynamic laser light scattering.

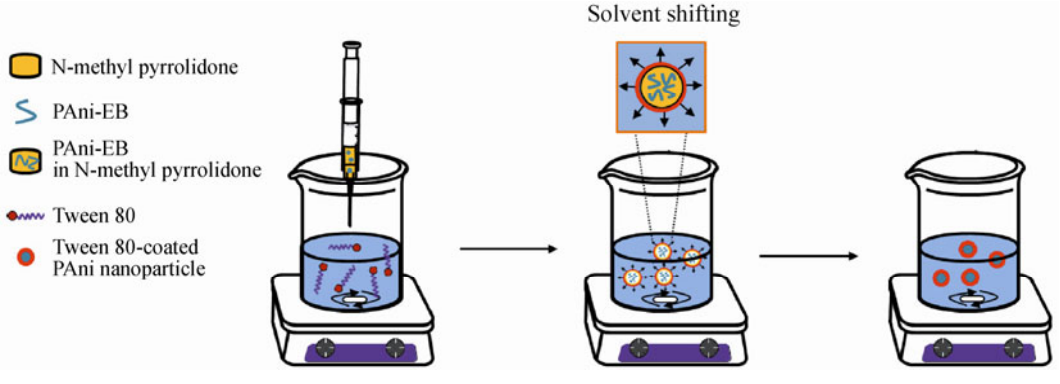

Scheme 1 Schematic illustration of the preparation of water-soluble PAni nanoparticles coated by Tween 80 using a solvent-shift method.

As the feed amount of PAni was decreased, the size of the resultant nanoparticles decreased from 26.4 ± 3.7 nm with 300 mg of PAni, to 125.2 ± 24.9 nm with 100 mg of PAni, and to 96.9 ± 21.2 nm with 50 mg of PAni. However, these relatively large TPAni nanoparticles demonstrated poor colloidal stability in aqueous solution. Thus, a lower feed mass of 10 mg of PAni was used, which resulted in smaller (44.6 ± 10.6 nm) and more stable TPAni nanoparticles (Fig. 1(a)). We also confirmed the solubility of bare PAni in various solvents. In the case of deionized water, the bare PAni precipitated in the solution, and in the case of chloroform, the bare PAni nanoparticles had larger size and poorer solubility than in NMP (Fig. S1(a) in the Electronic Supplementary Material (ESM)). Furthermore, the solubilities of TPAni nanoparticles were higher those of bare PAni in deionized water, chloroform, and NMP (Figs. S1(b) and S1(c) in the ESM). Moreover,

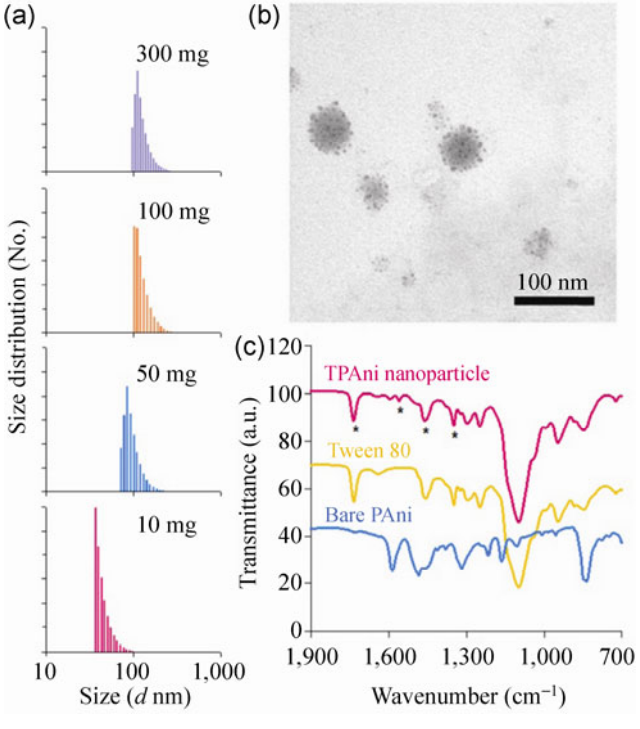

Figure 1 Characterization of TPAni nanoparticles. (a) Size distributions of TPAni nanoparticles after varying the feed amounts of PAni in the EB state (300, 100, 50, and 10 mg). (b) Transmission electron microscope (TEM) image of TPAni nanoparticles (feed amount: 10 mg of PAni). (c) Fourier transform infrared spectroscope (FT-IR) spectra of TPAni nanoparticles (upper), Tween 80 (medium), and bare PAni (lower). Asterisks represent interesting peaks described in more detail in the text.

we also prepared TPAni nanoparticles by varying the feed amounts of Tween 80 from 0 mg to 500 mg (Fig. S2 in the ESM). As the feed amounts of Tween 80 were increased, the size of TPAni nanoparticles decreased, but with 500 mg of Tween 80, the size of the resulting TPAni nanoparticles was over 1 μm because of aggregation of each TPAni nanoparticle. These results suggest that the size and stability of TPAni nanoparticles are predominantly affected not by the amount of Tween 80 but by the amount of PAni. A transmission electron microscopy image of TPAni nanoparticles shows the spherical morphology of the final nanoparticles (Fig. 1(b)). The high electron density of the PAni structure from the benzenoid and quinoid groups enabled TPAni nanoparticles to be observed without any staining steps. The chemical structure of TPAni was confirmed by peaks in the Fourier transform infrared spectra: 1,738 cm^{-1} (C=O from ester groups of Tween 80), 1,330 cm^{-1} (aromatic C–N stretching), 1,467 cm^{-1} (C=C and C=N stretching of benzenoid rings), and 1,563 cm^{-1} (C=C and C=N stretching of quinoid rings) (Fig. 1(c)). Collectively, these results confirm that small and stable TPAni nanoparticles can be fabricated by the solvent-shift method without requiring an additional energy-intensive process.

To investigate the influence of doping on the colorimetric potential, TPAni nanoparticles were doped with hydrogen chloride (HCl). Changes in the optical properties of TPAni nanoparticles due to protonation (with variation of HCl concentration from 10^{-1} to 10^{-10} M) were observed. Figure 2(a) shows the effects of HCl concentration on the colorimetric properties of TPAni nanoparticles. At high HCl concentrations (> 10^{-2} M), TPAni nanoparticles transitioned to an emeraldine salt (ES, green color) state. At lower HCl concentrations (< 10^{-3} M), TPAni nanoparticles transitioned to an EB state (blue color). Here, TPAni nanoparticles were not aggregated or precipitated under any pH conditions. Figure 2(b) shows the absorbance spectra (2120UV Mecasys, Korea) of TPAni nanoparticles over a range of HCl concentration. At 10^{-1} M HCl concentration, TPAni nanoparticles were in the doped state (ES), as indicated by the presence of the π–π* transition of the benzenoid rings as well as polaron bands transitions at about 2.95 and

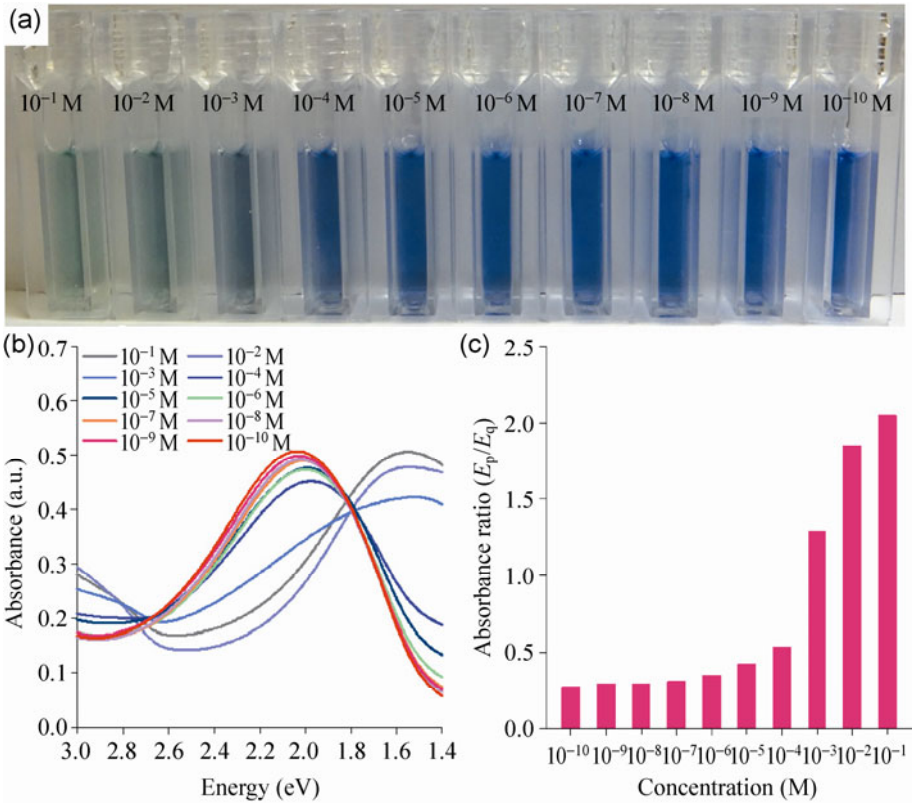

Figure 2 The colorimetric properties of TPAni nanoparticles as a function of varying HCl concentration. (a) Photographs, (b) absorbance spectra, and (c) absorbance ratios (E_p/E_q) for TPAni nanoparticles (0.005 mg/mL) at various HCl concentrations.

1.20–1.55 eV [21]. With decreasing HCl concentration, the polaron bands at 2.95 and 1.20–1.55 eV gradually decreased in intensity, and a strong absorbance band at about 2.07 eV was observed. The absorbance band at 2.07 eV is attributed to excitation from the highest occupied molecular orbital of the three-ring benzenoid part of the system to the lowest unoccupied molecular orbital of the localized quinoid ring and the two surrounding imine nitrogens in the EB state of the PAni nanoparticles [22]. In order to distinguish more specifically between the EB and ES doped states of TPAni nanoparticles, the absorbance ratios (E_p/E_q, p: polaron band, q: quinoid ring) were calculated at representative energies of the peaks for the EB (E_q) and ES (E_p) states (Fig. 2(c)). As the HCl concentration decreased from 10^{-1} to 10^{-7} M, the absorbance ratio also decreased, but it did not change further at lower HCl concentrations ($< 10^{-7}$ M). These results indicate that the spectral changes of TPAni nanoparticles can be used to determine the specific redox state of a biological system. These results also indicate that TPAni nanoparticles can be doped with H^+ ions and their counter-ions. As a result, the localized polaron transition and π–π* transition of the benzenoid ring are observed in the ES state. These transitions have specific peaks in the absorbance spectrum. For the localized polaron transition, a broad peak at 1.20–1.55 eV was observed, and in the case of the π–π* transition of the benzenoid ring, an absorbance peak at 2.95 eV was observed. Moreover, as the concentration of H^+ ions decreased, the localized quinoid ring structure and the two surrounding imine nitrogens of the EB state were observed. Due to this structural transition of PAni, a strong absorbance peak at 2.07 eV is observed. As a result of these changes in absorption peaks, the valley of the absorbance spectra also changed as shown in Fig. 2(b). Generally, objects can be said to have the color of light leaving their surfaces, that is, the human eye can perceive the color of objects by receiving the reflected wavelengths of light from the

object. Accordingly, we analyzed the valley of the absorbance spectra for each state of PAni, because the wavelength of the valley is correlated with the reflected light from PAni. The wavelength of the valley in the ES state is about 2.58 eV, and for the EB state, the wavelength of the valley is about 2.95 eV. As the wavelength of valley is changed, the color of PAni solution also changes. As a result, the TPAni nanoparticles in the ES state exhibit a green color, whilst in the case of the EB state, the color is blue. Using this sensitive colorimetric sensing capability of TPAni nanoparticles for H^+ ions, they can be used to determine the redox state of biological systems because the transfer of H^+ ions can be detected using these TPAni nanoparticles. In the doping process for PAni (Fig. S2 in the ESM), H^+ ions and their counter-ions play a dominant role. In other words, the doped state of PAni means that PAni receives H^+ ions from other materials or biological systems, and these H^+ ions are one of the materials participating in redox reactions. TPAni nanoparticles as a nanoprobe can sense various received dopants including lactic acid, pyruvic acid, and co-enzymes besides H^+ ions. Therefore, TPAni nanoparticles can be used to determine the specific redox state of a biological system.

In addition, TPAni nanoparticles were also characterized by cyclic voltammetry (CV) in order to investigate their electrochemical activity such as their redox potentials. As shown in Fig. S4 (in the ESM), three pairs of redox peaks were observed in the potential range of –0.2 to 1.0 V vs. a standard calomel electrode (SCE). The first pair of redox peaks (denoted as Ox 1 and Red 1) corresponds to the interconversion of the leucoemeraldine (fully reduced) form to the emeraldine form, the second pair of redox peaks (denoted as Ox 2 and Red 2) is due to the degradation of products (from hydroquinone to quinone) and the last pair of peaks (denoted as Ox 3 and Red 3) results from the oxidation of emeraldine to pernigraniline (the fully oxidized form).

To investigate the colorimetric probe ability of TPAni nanoparticles, doping capability was evaluated using various dopants. The majority of cancer cells live and proliferate based on the Warburg effect (aerobic glycolysis—glycolysis even under aerobic conditions) rather than oxidative phosphorylation in the mitochondria [23]. As a result, unlike most normal cells, cancer cells derive adenosine triphosphates as a metabolic fuel from uptaken glucose and produce pyruvate and lactate as metabolites [24]. Therefore, two representative biological dopants (here, lactic acid and pyruvic acid) were selected and the doping potential of TPAni nanoparticles was assessed. By treatment of lactic acid with TPAni nanoparticles, colorimetric features were revealed and a doped state was observed with 1 M lactic acid (Figs. 3(a) and 3(b)). In particular, for pyruvic acid, the absorbance spectra showed that TPAni nanoparticles became fully doped with pyruvic acid on increasing the pyruvic acid concentration (Figs. 3(c) and 3(d)). However, even at high concentrations of sodium chloride (NaCl) and fetal bovine serum (FBS), no aggregation of TPAni nanoparticles (Figs. 3(e) and 3(f)) or color changes were observed (Figs. 3(g) and 3(h)).

We subsequently evaluated the colorimetric capacity of TPAni nanoparticles as a redox indicator for live cancer cells. TPAni nanoparticles (0.1 mg/mL, 50 μL) were incubated with various statuses (live, fixation, and lysate) of MDA-MB-231 cells (5×10^6 cells/4.5 mL, respectively) for 48 h in order to observe colorimetrically any change from an EB to an ES state. There was no cellular toxicity at the concentration of TPAni nanoparticles employed (Fig. S5 in the ESM). As shown in Figs. 4 and S6 (in the ESM), TPAni nanoparticles successfully acted as redox indicators after incubation with proliferating live MDA-MB-231 cells. TPAni nanoparticles treated with live MDA-MB-231 cells exhibited a green color of the supernatant obtained from the cultured medium, whereas fixed and lysed cells exhibited blue colors. As shown in Fig. 4(b), TPAni nanoparticles treated with live MDA-MB-231 cells exhibited a polaron band at about 1.20–1.55 eV and a quinoid ring band at 2.07 eV with fixed and lysed MDA-MB-231 cells. Moreover, the absorbance ratio (E_p/E_q) was ca. 2 times and 1.75 times larger for TPAni nanoparticles treated with live MDA-MB-231 cells compared with the corresponding values obtained with fixed and lysed cells, respectively (Fig. 4(c)). In order to obtain more specific details about biological dopants with TPAni nanoparticles, we assessed the color of the cells treated with TPAni nanoparticles. As shown in Fig. 4(d), TPAni nanoparticles were taken up

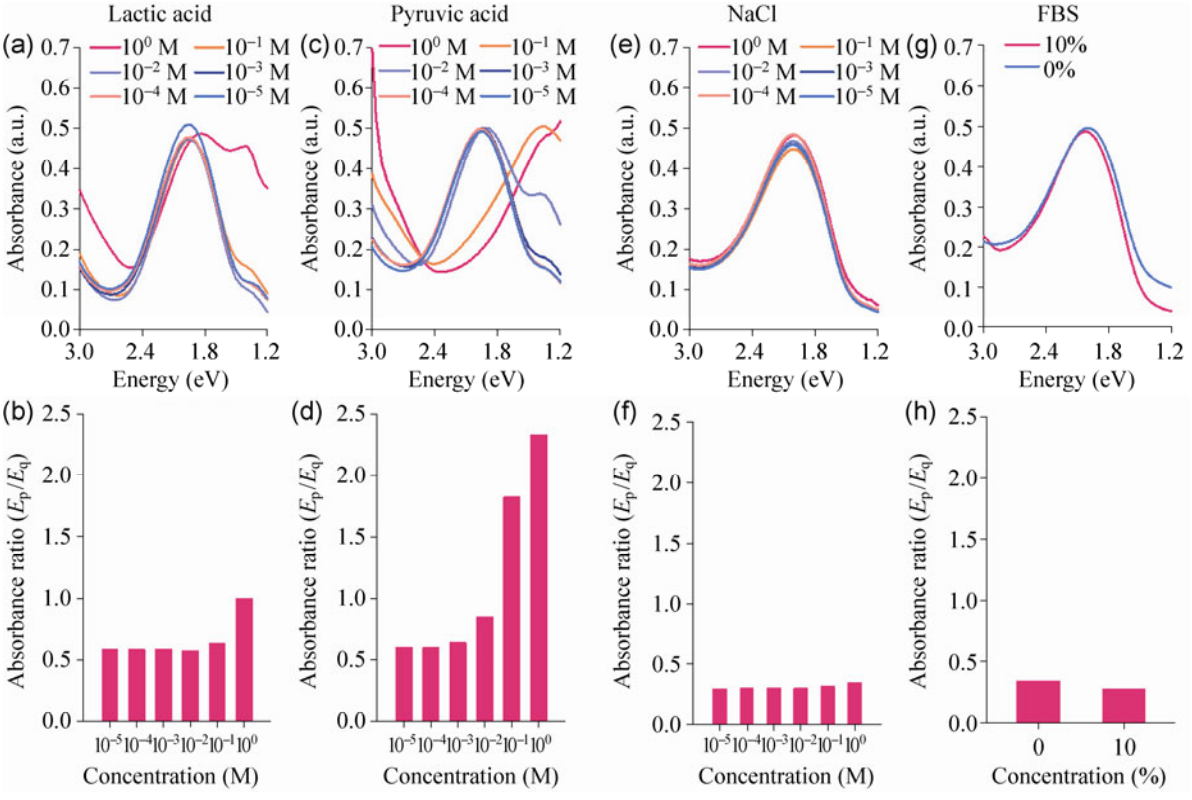

Figure 3 The colorimetric ability of TPAni nanoparticles with various biological dopants. Absorbance spectra and absorbance ratios (E_p/E_q) of TPAni nanoparticles (0.005 mg/mL) treated with (a) and (b) lactic acid, (c) and (d) pyruvic acid, (e) and (f) NaCl, and (g) and (h) FBS.

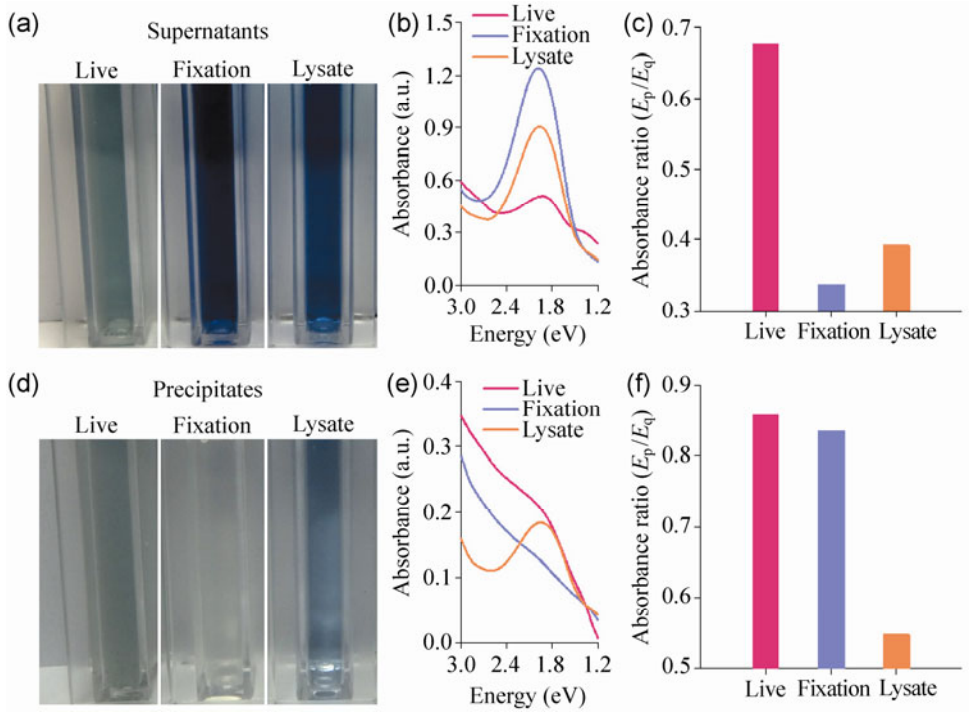

Figure 4 The colorimetric capability of TPAni nanoparticles with various statuses of cancer cells. (a) Photographs, (b) absorbance spectra, and (c) absorbance ratios (E_p/E_q) for supernatants from cell cultured media after treatment with TPAni nanoparticles (0.01 mg/mL) under the indicated conditions. (d) Photographs, (e) absorbance spectra, and (f) absorbance ratios (E_p/E_q) for precipitates from cell cultured media after treatment with TPAni nanoparticles (0.01 mg/mL) under the indicated conditions.

by MDA-MB-231 cells, therefore, TPAni nanoparticles treated with live MDA-MB-231 cells were affected by intracellular biological dopants such as pyruvic acid, and an increased polaron band intensity at 1.20–1.55 eV was observed as shown in Fig. 4(e). However, for the fixed MDA-MB-231 cells, the color of cells remained unchanged, showing that TPAni nanoparticles could not penetrate into the cells. Furthermore, the lysed MDA-MB-231 cells exhibited a blue color, characteristic of the EB state of TPAni nanoparticles, confirming that the cells had been broken down. We also analyzed absorbance spectra and absorbance ratios of the cells in each case. As mentioned earlier, in the case of the lysed MDA-MB-231 cells, the cellular structure was decomposed and the absorbance spectrum was similar to the EB state of TPAni nanoparticles (Fig. 4(e)). In the case of the live MDA-MB-231 cells, a slight increase in the intensity of the broad band at 1.77–2.07 eV was observed (Fig. 4(b)). This means that TPAni nanoparticles were taken up by MDA-MB-231 cells, so TPAni nanoparticles can be used to distinguish between the statuses of cells by means of its uptake efficiency. For a more specific classification, we also calculated the absorbance ratio in each case (Fig. 4(f)). The live MDA-MB-231 cells had the highest value. During cancer cell metabolism, redox stress induced by the Warburg effect increases the concentration of metabolites—such as pyruvic acid, lactic acid and co-enzymes—that can act as biological dopants [25]. Thus, the confined active doping effect from live cancer cells may prove to be a crucial factor in the doping of TPAni nanoparticles. It is also known that the transition from the EB state to the ES state of TPAni nanoparticles requires dopants [26]. Therefore, we speculate that biological dopants generated by proliferating cancer cells may result in the conversion of the doped state of TPAni nanoparticles.

In summary, we have formulated redox-sensitive nanoprobes based on PAni using a solvent-shift method. The solvent-shift method is simple and quick and allows fabrication of water-stable TPAni nanoparticles without any additional energy input. The TPAni nanoparticles formed stable small colloids in aqueous solution without any aggregation or precipitation. Moreover, TPAni nanoparticles could be doped by biological dopants. The resulting colorimetric changes allowed TPAni nanoparticles to recognize the redox activity and energetic process of live cancer cells.

Experimental

Synthesis of PAni: PAni was synthesized by a chemical oxidation polymerization method using a previously published protocol. In detail, PAni in the EB state was synthesized in the presence of excess HCl with ammonium persulfate as the oxidant. Aniline monomer (0.2 mol) was added to a 1 M HCl aqueous solution (300 mL). Polymerization was conducted by the dropwise addition of ammonium persulfate (0.05 mol) solution prepared in 200 mL of a 1 M HCl aqueous solution as an oxidant for 6 h at room temperature. The precipitated polymer salt was recovered from the reaction vessel by filtration and re-dispersed in a 1 M sodium hydroxide solution (500 mL). The deprotonated EB was then filtered and re-dispersed in acetone (500 mL). Finally, EB was obtained as a fine powder after filtration and drying in a vacuum oven for 48 h.

Preparation of TPAni nanoparticles: TPAni nanoparticles were prepared by a solvent-shift method using Tween 80. First, 10 mg of PAni in the EB state dissolved in 1.5 mL N-methyl-2-pyrrolidinone was added to 20 mL aqueous solution containing 200 mg of Tween 80. The mixture was vigorously stirred at room temperature for 24 h. After the reaction, TPAni nanoparticles were purified by centrifugation (15,000 rpm for 30 min) three times, and the precipitated TPAni nanoparticles were dispersed in deionized water.

Characterization: The size distribution of TPAni nanoparticles was first determined using dynamic laser scattering (ELS-Z, Otsuka, Japan) and confirmed by transmission electron microscopy (JEM-1011 JEOL, Japan). Fourier transform infrared analysis (Bruker) was used to investigate the chemical structure of TPAni nanoparticles. All absorbance spectra were acquired with a UV–Vis spectrometer (2120UV Mecasys, Korea).

***In vitro* assay:** The breast cancer cell line MDA-MB-231 (ATCC) was seeded at a density of 1×10^6 cells/dish on to a 100 mm × 20 mm cell culture dish and incubated for 24 h at 37 °C. Paraformaldehyde was used for cell fixation and a radioimmunoprecipitation assay buffer

was used for cell lysis. Subsequently, 4.5 mL of each cell culture medium (live, fixed, and lysed MDA-MB-231 cells) was treated with 0.5 mL of TPAni nanoparticles (0.1 mg/mL) and incubated for 48 h. For the preparation of supernatants and precipitates, incubated cancer cells were collected from the cell culture dish and centrifuged (1,000 rpm, 3 min). After the centrifugation, the supernatants and precipitates were collected separately for further experiments.

Acknowledgements

This work was supported by the National Research Foundation of Korea (NRF) Grant funded by the Korea government, Ministry of Education, Science Technology (MEST) (Nos. 2010-0023202, 2012R1A2A1A01011328, and 2012050077), and by a grant of the Korea Health technology R&D Project, Ministry of Health & Welfare, Republic of Korea (No. A121986).

Electronic Supplementary Material: Supplementary material (photographs of TPAni nanoparticles solutions for solubility tests (Fig. S1), size distribution of TPAni nanoparticles after varying the feed amounts of Tween 80 (Fig. S2), chemical structures of PAni in an EB and ES states (Fig. S3), cyclic voltammograms of TPAni nanoparticles (Fig. S4), cell viability tests (Fig. S5), and the colorimetric capability of TPAni nanoparticles with normal cells (Fig. S5)) is available in the online version of this article at http://dx.doi.org/10.1007/s12274-013-0312-z.

References

[1] Gustafsson, G.; Cao, Y.; Treacy, G. M.; Klavetter, F.; Colaneri, N.; Heeger, A. J. Flexible light-emitting diodes made from soluble conducting polymers. *Nature* **1992**, *357*, 477–479.

[2] Liu, W.; Kumar, J.; Tripathy, S.; Senecal, K. J.; Samuelson, L. Enzymatically synthesized conducting polyaniline. *J. Am. Chem. Soc.* **1998**, *121*, 71–78.

[3] Wang, Y.; Wang, X.; Li, J.; Mo, Z.; Zhao, X.; Jing, X.; Wang, F. Conductive polyaniline/silica hybrids from sol–gel process. *Adv. Mater.* **2001**, *13*, 1582–1585.

[4] Li, D.; Huang, J. X.; Kaner, R. B. Polyaniline nanofibers: A unique polymer nanostructure for versatile applications. *Acc. Chem. Res.* **2009**, *42*, 135–145.

[5] D'Arcy, J. M.; Tran, H. D.; Tung, V. C.; Tucker-Schwartz, A. K.; Wong, R. P.; Yang, Y.; Kaner, R. B. Versatile solution for growing thin films of conducting polymers. *Proc. Natl. Acad. Sci. U. S. A.* **2010**, *107*, 19673–19678.

[6] Kamikawa, T. L.; Mikolajczyk, M. G.; Kennedy, M.; Zhang, P.; Wang, W.; Scott, D. E.; Alocilja, E. C. Nanoparticle-based biosensor for the detection of emerging pandemic influenza strains. *Biosens. Bioelectron.* **2010**, *26*, 1346–1352.

[7] Gowda, S. R.; Leela Mohana Reddy, A.; Zhan, X. B.; Ajayan, P. M. Building energy storage device on a single nanowire. *Nano Lett.* **2011**, *11*, 3329–3333.

[8] Ma, Y. F.; Zhang, J. M.; Zhang, G. J.; He, H. X. Polyaniline nanowires on Si surfaces fabricated with DNA templates. *J. Am. Chem. Soc.* **2004**, *126*, 7097–7101.

[9] Sun, Q. H.; Bi, W.; Fuller, T. F.; Ding, Y.; Deng, Y. Fabrication of aligned polyaniline nanofiber array via a facile wet chemical process. *Macromol. Rapid Commun.* **2009**, *30*, 1027–1032.

[10] Anilkumar, P.; Jayakannan, M. Hydroxyl-functionalized polyaniline nanospheres: Tracing molecular interactions at the nanosurface via vitamin C sensing. *Langmuir* **2008**, *24*, 9754–9762.

[11] Jin, E.; Wang, X.; Liu, N.; Zhang, W. J. Self-assembled microspheres of glucose-containing polyaniline by alkali-guided method. *Mater. Lett.* **2007**, *61*, 4959–4962.

[12] Horn, D.; Rieger, J. Organic nanoparticles in the aqueous phase—theory, experiment, and use. *Angew. Chem. Int. Ed.* **2001**, *40*, 4330–4361.

[13] Barthet, C.; Armes, S. P.; Lascelles, S. F.; Luk, S. Y.; Stanley, H. M. E. Synthesis and characterization of micrometer-sized, polyaniline-coated polystyrene latexes. *Langmuir* **1998**, *14*, 2032–2041.

[14] Riede, A.; Helmstedt, M.; Riede, V.; Stejskal, J. Polyaniline dispersions. 9. dynamic light scattering study of particle formation using different stabilizers. *Langmuir* **1998**, *14*, 6767–6771.

[15] Zhang, L.; Wan, M. Self-assembly of polyaniline—from nanotubes to hollow microspheres. *Adv. Funct. Mater.* **2003**, *13*, 815–820.

[16] Neelgund, G. M.; Oki, A. A facile method for the synthesis of polyaniline nanospheres and the effect of doping on their electrical conductivity. *Polym. Int.* **2011**, *60*, 1291–1295.

[17] Yang, J.; Choi, J.; Bang, D.; Kim, E.; Lim, E. K.; Park, H.; Suh, J. S.; Lee, K.; Yoo, K. H.; Kim, E. K. et al. Convertible organic nanoparticles for near-infrared photothermal ablation of cancer cells. *Angew. Chem. Int. Ed.* **2011**, *50*, 441–444.

[18] Bilati, U.; Allémann, E.; Doelker, E. Development of a

nanoprecipitation method intended for the entrapment of hydrophilic drugs into nanoparticles. *Eur. J. Pharm. Sci.* **2005**, *24*, 67–75.

[19] Aubry, J.; Ganachaud, F.; Cohen Addad, J. P.; Cabane, B. Nanoprecipitation of polymethylmethacrylate by solvent shifting: 1. Boundaries. *Langmuir* **2009**, *25*, 1970–1979.

[20] Yang, J.; Lee, E. S.; Noh, M. Y.; Koh, S. H.; Lim, E. K.; Yoo, A. R.; Lee, K.; Suh, J. S.; Kim, S. H.; Haam, S. et al. Ambidextrous magnetic nanovectors for synchronous gene transfection and labeling of human MSCs. *Biomaterials* **2011**, *32*, 6174–6182.

[21] Huang, W. S.; MacDiarmid, A. G. Optical properties of polyaniline. *Polymer* **1993**, *34*, 1833–1845.

[22] Huang, J. X.; Kaner, R. B. The intrinsic nanofibrillar morphology of polyaniline. *Chem. Commun.* **2006**, 367–376.

[23] Vander Heiden, M. G.; Cantley, L. C.; Thompson, C. B. Understanding the Warburg effect: The metabolic requirements of cell proliferation. *Science* **2009**, *324*, 1029–1033.

[24] Cairns, R. A.; Harris, I. S.; Mak, T. W. Regulation of cancer cell metabolism. *Nat. Rev. Cancer* **2011**, *11*, 85–95.

[25] Stubbs, M.; McSheehy, P. M. J.; Griffiths, J. R.; Bashford, C. L. Causes and consequences of tumour acidity and implications for treatment. *Mol. Med. Today* **2000**, *6*, 15–19.

[26] Tao, S.; Hong, B.; Kerong, Z. An infrared and Raman spectroscopic study of polyanilines co-doped with metal ions and H^+. *Spectrochim. Acta A* **2007**, *66*, 1364–1368.